J Mater Sci (2022) 57:12810–12823

Chemical routes to materials

Advantageous optical characteristics of tantalum vanadium oxide as counter electrode in electrochromic devices

Mario Gies[1,2,*], Thomas Rempel[1,2], Martin Becker[1,2], and Angelika Polity[1,2]

[1] Institute for Experimental Physics I, Justus Liebig University, 35392 Giessen, Germany
[2] Center for Materials Research (LaMa), Justus Liebig University, 35392 Giessen, Germany

Received: 14 March 2022
Accepted: 2 June 2022
Published online: 5 July 2022

ABSTRACT

Smart windows are an important technology in terms of energy saving potential in the building sector due to their ability to control visible light and thermal radiation. The essential component of this type of window glazing is an electrochromic thin film. In addition to the widely established tungsten oxide as the optically active material, in particular the counter electrode offers significant potential for improving the overall device performance. In this study, tantalum vanadium oxide films are prepared by reactive radio-frequency sputtering on fluorine-doped tin oxide substrates and optimized in terms of their spectro-electrochemical properties as ion storage layer. We show that an oxide-based tantalum-vanadium alloy is a promising approach to address the open challenges of pure vanadium pentoxide. The coatings exhibit color neutrality in combination with a high transmittance of up to 80% in the as-prepared state and suitable optical transmittance switching. Additionally, we find both a sufficient stability upon cycling and a suitable charge density of about 35 mC cm^{-2}. Thus, the presented oxide-based alloy offers a beneficial performance as an ion storage layer in electrochromic devices.

Introduction

Global population growth and the associated increase in energy demand over the last decades amplify the need for rising energy production [1]. At the same time, global climate change raises the question of an alternative, sustainable energy generation and its efficient use and conservation. This requires perpetual improvement of existing techniques and the simultaneous development of new technologies. In this context, the building sector represents a significant sphere of action towards energy saving [2, 3]. One way to save energy in this sector is the

Handling Editor: Pedro Camargo.

Address correspondence to E-mail: Mario.Gies@exp1.physik.uni-giessen.de

https://doi.org/10.1007/s10853-022-07408-0

technology of electrochromic smart windows. These allow the control of light and heat radiation entering the building, adapted to the particular needs. The basic component of such window glazing consists of a specific system of thin layers, namely two electrodes, separated from each other by an ion conducting electrolyte. Typically, the latter either consists of an organic liquid or polymer gel or is given by an oxide layer [4–7]. An electrochromic material is used as the optically active electrode. In combination with an external voltage source, it is able to modulate its optical state depending on the applied electrical voltage. By selectively changing the electrical voltage, ions are inserted (intercalated) into the electrochromic layer through the adjacent electrolyte layer and change the optical state of this material. Tungsten oxide is by far the most widely established electrochromic electrode material, as it exhibits strong coloration during ion intercalation, *i.e.*, cathodic electrochromism [8–10]. Studies on this material started as early as in the late 1960s by S. K. Deb [11, 12]. The general reversible electrochromic behavior is due to the formation of M_xWO_{3-y}, where M corresponds to H, Li, etc., and where metal ion insertion and electron injection result in an intense blue color with low x value due to photoaffected intervalence charge transfer. Extensive studies show that the intercalation–deintercalation-based electrochromic performance depends mainly on the ion intercalation reaction, which itself is determined by the material's crystallinity, doping level and microstructure, among others [13–16]. Increasing the color tunability of WO_{3-y}-based electrochromic devices is another key issue, which is of growing interest over the last few years. Here, different approaches are pursued to combine functional materials to yield multifunctional and tunable electrochromism [17–20].

Besides tungsten oxide, there are plenty other electrochromic materials [20, 21]. Among them, transition metal oxides play a special role, as there are those like WO_{3-y}, which exhibit cathodic electrochromism, and those like Ni oxide and Ir oxide are anodic electrochromic materials, thus showing a change in their optical state from transparent to a neutral colored state upon extraction of H, Li, etc. [10, 22–24]. Naturally, to achieve the highest possible electrochromic efficiency, high optical modulation, as well as good cyclic reversibility of the entire layer system, it is advantageous if such an anodic electrochromic material is complemented with the cathodic WO_{3-y} film [25, 26]. However, the anodic oxide film may suffer severe charge capacity degradation on extended electrochemical cycling in WO_{3-y}-based device. Hence, over the last decades, investigations on counter electrodes have been extensive to overcome this issue. As already mentioned, the counter electrode may exhibit electrochromic properties; however, it serves primarily as an ion storage layer. Thus, another feasible strategy is to use an optically passive counter electrode acting as a pure ion storage layer. Here, in addition to beneficial optical properties, the ability of storing a sufficient amount of charge is also required. This amount of charge is, of course, highly dependent on the optically active electrode used in the overall electrochromic device. For example, if it has a high coloration efficiency, the amount of charge involved in the (de-)coloration will be reduced. In case of tungsten oxide as the electrochromic cathode, the required amount of charge may differ significantly and, in optimized systems, will be in the order of 15–35 mC cm^{-2} [27, 28]. Therefore, an ideal counter-electrode for tungsten oxide should combine an ion storage capacity above 35 mC cm^{-2}, an optical transmittance in the discharge state of at least 80% and only small variation in the optical transmittance of the film with charging.

The relationship between microscopic and macroscopic properties, materials and deposition parameters provides an important guidance to optimize characteristics for a given application. This is especially true for vanadium oxides, since these films may exhibit very different electrical and optical properties depending on the deposition technique used. Vanadium oxide can be present in different phases according to V_nO_{2n+1} (Magnéli phases) or V_nO_{2n-1} (Wadsley phases) [29], in which the oxidation states V^{2+}, V^{3+}, V^{4+} or V^{5+} are found. In terms of electrochromism, of particular interest is the vanadium pentoxide (V_2O_5). This material contains the highest oxidation state V^{5+}, which is associated with a yellowish color of the pristine material. V_2O_5 films can be deposited by several techniques, such as chemical vapor deposition [30–32], solgel process [33, 34], atomic layer deposition [35, 36], pulsed laser deposition [37] or sputter deposition [38–40], among others. Several studies have already been performed on sputtered V_2O_5 coatings, investigating the effects of different growth parameters, such as varying the oxygen content in the process gas or the growth

temperatures, on the electrochromic characteristics of thin films [41–43]. Due to its layered structure, V_2O_5 is a typical compound for intercalation mechanisms [44]. The electrochemical reaction in V_2O_5 thin films is described as a double injection of electrons and Li^+ cations into a V_2O_5 matrix, which takes place according to the following scheme [44, 45]:

$$V_2O_5 + xLi^+ + xe^- \leftrightarrow Li_xV_2O_5. \quad (1)$$

In this reaction, V_2O_5 undergoes several structural modifications, depending on the amount of intercalated Li^+ [46, 47]. Because of its suitable intercalation mechanism, V_2O_5 films have attracted considerable attention in recent decades and are considered as both, cathode or anode materials, for rechargeable lithium-ion batteries [36, 48–50]. Nevertheless, the limited long-term stability of such electrodes is a major challenge, which has been met by using different dopants [51–53].

In detail, V_2O_5 shows mixed anodic/cathodic (near UV range/near IR range) electrochromic behavior upon the intercalation process [54, 55]. The anodic electrochromic behavior is explained by a Burstein–Moss shift of the absorption edge, whereas the cathodic electrochromic behavior is rooted in the absorption of small polarons formed by changing V^{4+} valences [54]. In particular, the cathodic electrochromic switching characteristic, which dominates in the visible spectral range, counteracts the straightforward use of V_2O_5 as counter electrodes material. In this context, the optical impression of V_2O_5 changes from its yellow initial state to a bluish coloration; occasionally, a green or green-gray color impression is also reported [55–57]. Thus, changing the optical transmittance towards an increased color neutrality is of foremost interest. Additionally, however, the long-term stability of the material in terms of electrochemical cyclability must not be compromised. In order to achieve this aim, various studies have considered doping V_2O_5. Elements used include Ce [58–60], Cr [61], Fe [62], Mo [63–66], Nb [61, 67–70], Ta [68–72], Ti [38, 59, 73–75], or W [76]. Especially, the studies by Avellaneda et al. concerning the fundamental suitability of V_2O_5:Ta for use as counter electrodes are striking, as only small amounts of tantalum (2.5 und 5 mol%) were found to yield better long-term stability and higher charging capacity as compared to pure V_2O_5 [71, 72].

Here, we improve the ion storage capacity and stability of V_2O_5 by adding tantalum. In contrast to previous studies, we discuss samples sputtered from an Ta/V alloy target and, thus, the impact of higher amounts of tantalum. Aside from the required electrochemical stability, the optical properties are of primary interest. We evaluate the suitability of ternary tantalum vanadium oxide ($TaVO_x$) as counter electrode in an electrochromic device and show the superiority as compared with binary V_2O_5.

Experimental

The ternary $TaVO_x$ films are prepared by radio-frequency (rf) magnetron sputtering. The base pressure of the sputtering chamber is in the upper range of 10^{-7} mbar. We use a 4 in. V/Ta alloy target (V/Ta ratio of 50 at%/50 at%) with a purity of 99.5% from Kurt J. Lesker Company. Reactive sputtering is performed using a power density of 1.2 W cm^{-2} and an argon–oxygen gas mixture under a total gas flow of 50 sccm. In this work, we compare $TaVO_x$ thin films deposited with O_2/Ar ratios of 10/40 (20% O_2), 25/25 (50% O_2) and 40/10 (80% O_2). Both gases have a purity of 99.999%. K-Glass™ is used as substrate. To provide electrical contact for electrochemical measurements, the substrates are coated with a 300 nm thick fluorine-doped tin oxide (FTO) layer.

A Lambda 900 spectrometer from PerkinElmer Instruments is used to study the optical properties of the films in the as-deposited state. The surface structure is observed by scanning electron microscopy (SEM) using a Zeiss-Merlin setup.

The electrochromic properties of the coatings are investigated spectro-electrochemically. Electrochemical analyses are performed using an IviumStat potentiostat from Ivium Technologies. For electrochromic characterization, cyclic voltammetry (CV) measurements are recorded in a potential range between − 1.2 and 1.5 V with a potential sweep of 10 mV s^{-1}. Chronoamperometry (CA) is performed at a potential of − 1 or 1 V, applied for 10 min each. All electrochemical measurements are performed in the three-electrode configuration with a PECC-2 type cell of Zahner-Elektrik GmbH & Co. KG. Here, the as-deposited $TaVO_x$ layer serves as the working electrode. In addition, a platinum wire (counter electrode) and a leak-free Ag/AgCl reference electrode from Innovative Instruments, Inc. are used. The

electrolyte consists of 1 M dissolved lithium perchlorate ($LiClO_4$, purity of 99.99%, Sigma-Aldrich Chemie GmbH) in propylene carbonate (PC, anhydrous, Th. Geyer GmbH & Co. KG). In order to draw conclusions regarding the electrochromic properties, *in operando* optical measurements were realized with a spectrometer (tec5). The coloration efficiency (CE) serves as key measure to evaluate the electrochromic performance of the coatings:

$$\mathrm{CE} = \frac{\log_{10}\frac{T(\mathrm{b})}{T(\mathrm{c})}}{\mathrm{d}Q}, \tag{2}$$

here, the transmittance T in the bleached (b) and colored (c) states and the total charge density dQ involved are considered. We evaluate the coloration efficiency at a wavelength of 550 nm, as in this spectral range a very high sensitivity of the human eye is given.

Results and discussion

Optical and structural properties

Figure 1a shows transmittance measurements of rf-sputtered $TaVO_x$ thin films in the spectral range between 270 and 1000 nm. All samples were deposited under a total gas flow of 50 sccm of O_2/Ar mixture. They differ in the amount of reactive gas admixed to the gas flux. Here, the oxygen content varies between 20, 50 and 80%. To be comparable, all samples have a thickness of 100 nm. For the $TaVO_x$ samples studied, the overall transmittance obviously is independent of the gas composition during $TaVO_x$ deposition. However, compared to the pristine FTO-coated glass substrate (*cf.* gray curve in Fig. 1a), an additional absorption in the spectral range between 300 and 700 nm is observed. The absorption caused by the FTO substrate extends to a wavelength of 310 nm, whereas significant transmittance begins only at about 330 nm with an additional $TaVO_x$ layer. Hence, the overall transmittance in the violet spectral range is limited. For higher wavelengths, the transmittance rises to about 75% in the blue spectral range and finally above 75% in the remaining part of the visible spectrum. Furthermore, the transmittance only drops rather slowly in the near-infrared spectral range and stays above 70% for wavelengths up to 1000 nm. Overall, the deposited samples are not totally neutral in color and exhibit a pale yellowish color. The color fields in the legend of Fig. 1a illustrate the color impression of the respective sample. Note that there may exist different approaches to enhance the transmittance in the lower wavelength regime and, thus, yield a more neutral color impression, i.e., post-growth thermal annealing (*cf.* Figure S1 in the Supporting Information).

Next, we will discuss the structural properties of our as-deposited $TaVO_x$ thin films. Note that the samples were grown without using an additional

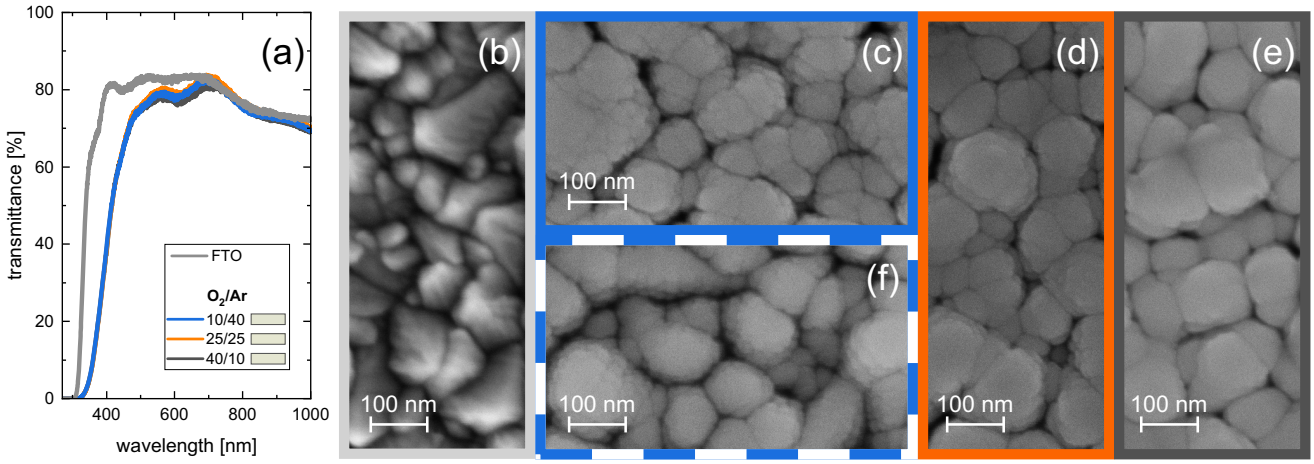

Figure 1 Transmittance measurements of 100 nm thick $TaVO_x$ samples prepared using different gas compositions during deposition (**a**). SEM images of the corresponding samples prepared under oxygen flux content of 20, 50 and 80% in the total process gas (**c–e**) in comparison with the pristine FTO coated glass substrate (**b**) and the 20% O_2 sample after 101 cycles of cyclic voltammetry (**f**).

substrate heating. Thus, all samples were amorphous, at least what can be deduced from X-ray diffraction (not shown here). Hence, we will restrict ourselves on discussing the samples' morphology observed by SEM measurements (*cf*. Fig. 1b–e). Fig. 1b provides information on the morphology of the FTO substrate used. Here, a fine-grained structure of arbitrary arrangement can be seen. Besides single grains of small size, the largest ones extend to a length of about 100–200 nm. Figure 1c–e illustrates the surfaces of $TaVO_x$ samples deposited under 20, 50 and 80% oxygen in the total gas mixture. The overall surface morphology of all $TaVO_x$ specimens is comparable. We find roundish grains of comparable size. The expansion of those grains is about 100 nm. Due to the grainy surface texture, some voids are visible and indicate a certain degree of porosity. This increase in material's surface allows for a pronounced ability to intercalate ions, which is required for the electrochromic application sought for. Furthermore, a decrease in oxygen content in the process gas leads to a certain roughening of the grainy structure, perceptibly by smaller features on top of the 100 nm sized grains. This is particularly evident for the sample with an oxygen content of 20% in the sputter gas (*cf*. Fig. 1c). Due to the missing reflections in X-ray diffraction and, thus, crystallinity of our $TaVO_x$ layer, we tentatively attribute the presence of the grains to the structure of the FTO substrate. Thus, the amorphous $TaVO_x$ may just adopt the crystalline features of the subjacent FTO.

Figure 1f shows the morphology of a $TaVO_x$ layer produced under oxygen-deficient conditions (20% oxygen), which has additionally passed the electrochemical test procedure consistent of 101 cycles of cyclic voltammetry followed by another intercalation step during chronoamperometry. Thus, the sample shown is intercalated with Li^+-ions. Compared to the as-prepared sample (*cf*. Fig. 1c), there are no significant changes in morphology to be seen. Hence, in the first instance, this suggests sufficient and suitable stability with regard to the cyclability of rf-sputtered $TaVO_x$ layer.

Electrochemical investigations

In the following, we investigate the switching behavior of the $TaVO_x$ samples and the corresponding electrochromic properties using cyclic voltammetry. In a first step, we analyze three samples of 100 nm thickness prepared with different process gas compositions: 20, 50 and 80% O_2 in the total gas flux, respectively. The measurement includes a total of eleven cycles and takes place in a potential range between −1.2 and 1.5 V *vs*. Ag/AgCl. To prevent irreversible phase transitions to occur at high intercalated amounts of Li^+ [46], the lower limit of the potential was fixed at the specified value of − 1.2 V. Figure 2a shows the evolution of the current density in the eleventh cycle of a voltammetry measurement of such samples. The cathodic current of the reduction starts at a potential between 0.5 and 0.6 V *vs*. Ag/AgCl for all samples shown. It can be seen that the initiation of this current drifts towards a lower potential for samples prepared with a higher oxygen content in the process gas. After the onset of the reduction current, it increases rapidly and leads to the formation of a first reduction peak. Again, a displacement of position can be observed in all samples. For samples prepared with a higher oxygen content in the process gas, this potential shifts towards a more negative value and is in the range of − 0.1 to 0.1 V *vs*. Ag/AgCl. An additional reduction peak can be seen at the lower end of the potential range. For the sample prepared under the lowest oxygen flow, the position is about − 1.1 V *vs*. Ag/AgCl. Due to the aforementioned drift of the reduction current, no fully developed reduction signal is evident for the other two thin films. Their second reduction feature is obviously outside the potential range chosen in this work. After reaching the reversal point of the potential at − 1.2 V *vs*. Ag/AgCl, a rapid increase into the positive range of the current density occurs. This indicates suitable switching kinetics of the $TaVO_x$ layers, since the accumulation of Li^+- ions starts immediately. Here, for samples prepared with low O_2/Ar ratio, the current density increases more rapidly in the low potential region. Nevertheless, an oxidation peak, corresponding to the reduction peak at − 1.1 V *vs*. Ag/AgCl, cannot be found due to the overlapping and smearing current signals. Note that the sample prepared under the highest oxygen flux clearly shows the lowest associated deintercalation current density in this particular potential range. However, this is attributed to the fact that the second reduction step was passed to the least extent in the potential range investigated. In contrast, the oxidation peak associated with the first reduction peak is evident for all samples. It is located between 0.1 and 0.2 V *vs*. Ag/AgCl and rapidly decreases with

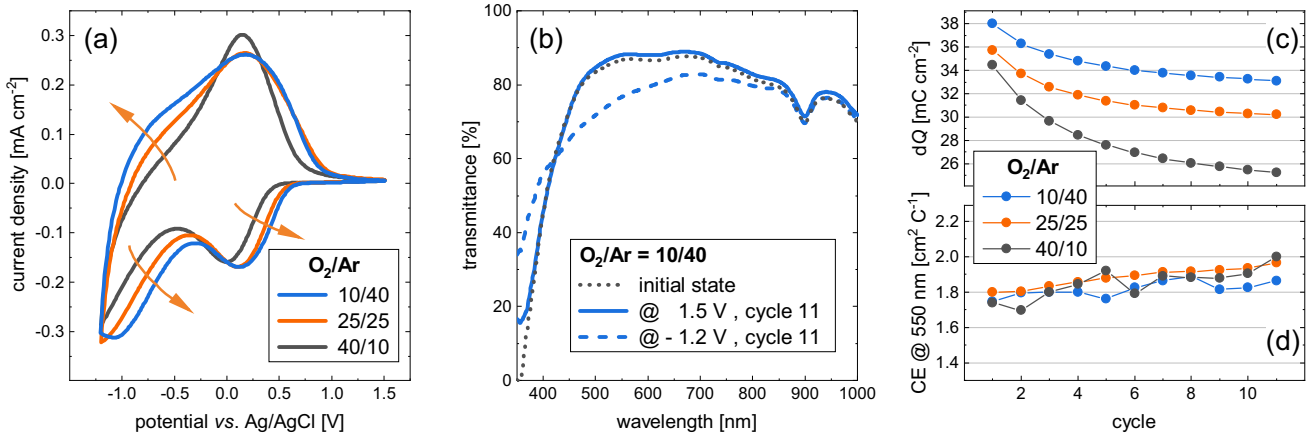

Figure 2 Eleventh cycle of CV measurements between −1.2 and 1.5 V *vs.* Ag/AgCl performed on 100 nm thick $TaVO_x$ films prepared at different O_2/Ar flux ratios in the process gas (**a**). Arrows in (**a**) indicate significant changes. Transmittance measurements of the initial state as well as the respective switching states at the reversal points of the potential in the eleventh CV cycle underline a good reproducibility for the sample with 20% O_2 (**b**). The charge density (d*Q*), involved within a cycle, and the associated coloration efficiency, referred to 550 nm at the maximally reduced/oxidized switching points, are shown in (**c**) and (**d**), respectively.

increasing positive potential. Finally, at the reversal potential of 1.5 V *vs.* Ag/AgCl the current density is almost infinitesimally small for all samples. In general, the cyclic voltammetry measurements shown in Fig. 2a emphasize that the sample prepared under the lowest oxygen flux shows the most suitable cyclic behavior, since both reduction steps are included in the potential range chosen. This indicates suitable stability with respect to their cyclability and switching kinetics. Note that a two-step reaction is also observed in the cyclization of pure V_2O_5, indicating different phase transitions in each case [45]. However, due to the lack of crystalline structure of the present $TaVO_x$ films, the reaction steps evident from the CV are not defined as sharp as compared to studies on crystalline V_2O_5 and are only present based on quite broad reduction and oxidation signals.

Figure 2b shows the transmittance measurements of the sample prepared under a low oxygen flux of 10 sccm (20% O_2) at different charge states with respect to Li^+ ions. Depicted are the intercalated state at −1.2 V *vs.* Ag/AgCl (dashed blue line) and the deintercalated state at 1.5 V *vs.* Ag/AgCl (solid blue line) of the eleventh cycle in comparison with the initial state after deposition (dotted gray line). With respect to the general switching properties, we find an electrochromic switching behavior, both anodic (between 350 and 420 nm) and cathodic (420 to 1000 nm). As mentioned before, this mixed anodic/cathodic electrochromic behavior is already known to exist from V_2O_5 [54, 55]. Thus, $TaVO_x$ exhibits an electrochromic switching behavior superior to that of V_2O_5 (*cf.* reference data in Figure S2 in the Supporting Information). In particular, in the deintercalated state we observe a striking transmittance as high as 85–90% across a large spectral range of the visible light. A disadvantage, however, is the relatively low transmittance in the violet and blue spectral range, which leaves a light beige color impression of our $TaVO_x$ layers. In this region, the Li^+ ion intercalated state also exhibits increased transmittance due to anodic electrochromic switching. In most of the visible spectral range, however, one loses transmittance due to cathodic electrochromic switching. In this case, the optical transmittance is about 70–80% and the layer is given a slightly brownish color appearance. Nevertheless, the $TaVO_x$ layers exhibit neither a greenish nor a bluish coloration, as one might expect for pure V_2O_5 coatings [55–57]. Therefore, a significant improvement in color neutrality of the intercalated optical state can be observed for our $TaVO_x$ samples. Finally, we need to compare the deintercalated state after eleven cycles with the initial optical state of the layer, i.e., before the actual CV measurement (dotted gray line). It is evident that both states show strong resemblance, indicating a suitable cyclability. If any, the transmittance of the Li^+ ion deintercalated state even exceeds that of the as-deposited sample. Thus, the layer was even slightly bleached in the course of the CV

measurement. We tentatively assign this effect to a certain degree of atomic rearrangement or healing of surface defects upon cycling.

In order to quantitatively study our $TaVO_x$ samples in terms of suitable electrochromic properties, we will assess two main key measures. These are the charge density dQ per cycle and the coloration efficiency CE with respect to 550 nm, as shown in Fig. 2c and d, respectively. The data points shown correspond to each out of eleven cycles of CV measurements performed in a potential range between − 1.2 and 1.5 V *vs.* Ag/AgCl as discussed in context with Fig. 2a.

First, we will discuss the charge density per cycle shown in Fig. 2c. For the material system under consideration and its application as an ion storage layer in an electrochromic cell, we aim at the highest possible capacity in terms of Li^+ ion storage capability. Based on the compared samples, it is evident that the ion storage capacity increases for samples grown with decreasing O_2 content in the process gas. Exemplarily, after the eleventh voltammetry cycle the corresponding charge density dQ for the sample prepared with an O_2/Ar ratio of 10/40 is about 33.1 mC cm^{-2}. In contrast, the charge density in the sample deposited with an O_2/Ar ratio of 40/10 is only 25.3 mC cm^{-2}. Previously, an increasing charge capacity has been observed in sputtered V_2O_5 films deposited under low-oxygen conditions [41]. The dependence of the capacity on the respective number of cycles passed and the associated curve is comparable for all three samples. The amount of charge involved in cycling is highest in the first cycle and decreases upon subsequent cycling. For the subsequent cycles, however, the capacity reduction decreases and a flattening of the curves can be seen. So we observe a saturation behavior and, thus, stabilization of the electrochromic properties. To emphasize this effect, we compare the ratio of the eleventh cycle capacity to that of the first cycle. The observed decrease in capacity is smaller for samples produced with low oxygen content in the process gas. Thus, after the eleventh cycle, the sample deposited with an O_2/Ar ratio of 40/10 has a capacity remaining of only 73.3%. In contrast, after the eleventh cycle, the sample prepared under low oxygen conditions (O_2/Ar ratio = 10/40) has a capacity remaining of 87.1%, which yields a charge density of 33.1 mC cm^{-2} in the eleventh cycle. Hence, we conclude that our $TaVO_x$ samples prepared with low oxygen flux gain stable switching characteristics after only a few cycles.

As the $TaVO_x$ layer is designed to act as a counter electrode or ion storage layer and exhibits cathodic electrochromic coloration over a broad visible spectral range, not only a suitable charge transfer is needed, but also distinct coloration efficiency requirements. Figure 2d shows the dependence of the coloration efficiency measured at a wavelength of 550 nm on the cycle number. Comparing the different samples, no trend is observed. In general, the coloration efficiencies range from 1.7 to 2.0 cm^2 Q^{-1}. A slight increase in coloration efficiency can be seen simultaneously with cycling; however, the coloration efficiency for all samples stays rather low. Due to the cathodic electrochromic switching characteristic in the spectral range considered, small values of the coloration efficiency are preferable for the material of $TaVO_x$. Thus, based on the charge density dQ per cycle and the coloration efficiency CE with respect to 550 nm, we select an O_2/Ar ratio of 10/40 for further studies, as we obtain the highest charge density dQ per cycle and the fastest stabilization of the switching characteristics for such layers.

Next, we vary the thickness of the $TaVO_x$ layer deposited with an O_2/Ar ratio of 10/40. We chose thicknesses between 75 and 300 nm on one hand to assure a closed layer without pinholes and to avoid large parts of $TaVO_x$ not participating in the electrochromic switching on the other hand. Figure 3a shows the current density transferred during cycling for the $TaVO_x$ layers of different thickness. We observe reduction features in the range of − 0.1 to 0.1 V *vs.* Ag/AgCl and at the lower end of the potential range at −1.2 V *vs.* Ag/AgCl, as well as an oxidation peak associated with the first reduction peak between 0.1 and 0.5 V *vs.* Ag/AgCl. Thus, in general we observe the same features already discussed in context with Fig. 2a. However, there are significant changes connected with the different thickness of the $TaVO_x$ layer. The behavior of the samples with a film thickness of 75 and 100 nm, respectively, is quite comparable and has already been described in some detail before. Due to the increasing ability to store charge, the corresponding area increases with increasing layer thickness. However, the voltammograms of the two thicker samples differ in shape compared to the thinner ones. It can be seen that both reduction signals are shifted towards lower potentials. The corresponding oxidation

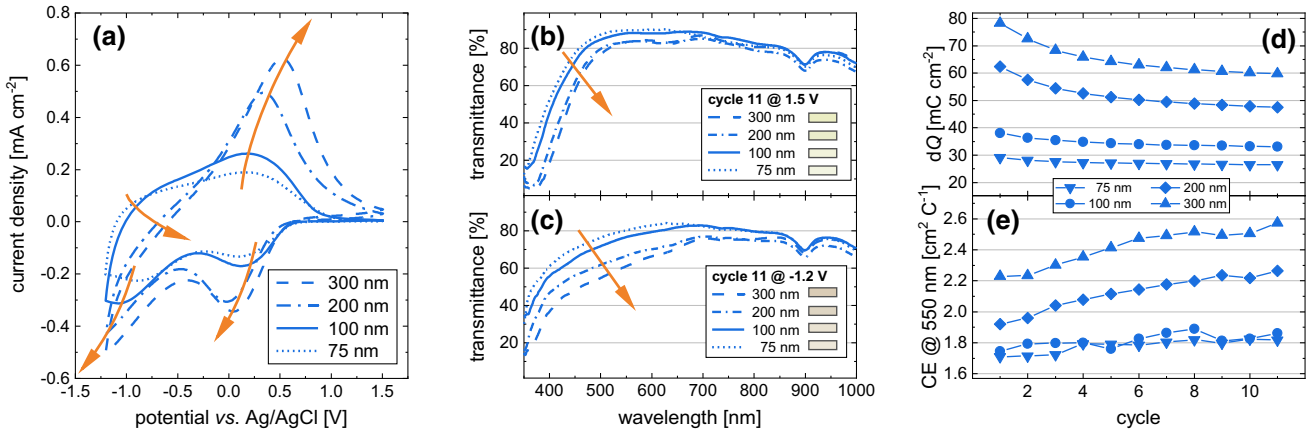

Figure 3 Eleventh cycle of CV measurements between −1.2 and 1.5 V *vs.* Ag/AgCl performed on $TaVO_x$ films of different thickness (**a**) and the corresponding transmittance measurements performed at the reversal points of the potential in the eleventh CV cycle (**b**,**c**). All films were deposited with an O_2/Ar ratio of 10/40. Arrows in (**a**–**c**) indicate significant changes induced by an increase in thickness. Charge density (**d**) and the associated coloration efficiency at 550 nm (**e**) in dependence on the cycle number and the $TaVO_x$ film thickness (different symbols).

signals shift with respect to their position to higher potentials. For both shifts, *cf.* arrows in Fig. 3a. In addition, the shift causes that the second reduction signal is no longer completely in the region of consideration and thus to be partially cut off. At the reversal point of the negative potential, the current density increases relatively slowly. This is based on the oxidation not taking place due to the missing second reduction step as described earlier. Accordingly, we observe a very low associated deintercalation current in the negative potential range for samples of 200 nm thickness and above and, thus, poorer switching kinetics. On the one hand, the chosen potential range is not large enough to sufficiently pass through both reduction states. On the other hand, for the deintercalation step, we observe a delayed oxidation process. Consequently, the samples with a thickness of 75 or 100 nm seem to be more suitable due to their better switching properties.

An additional drawback of an increased thickness of the $TaVO_x$ layer is apparent when it comes to the transmittance of the layer system $TaVO_x$ | | FTO | | glass. Thus, an increased overall thickness will intrinsically lower the transmittance. This holds true for both switching states, *cf.* Fig. 3b and c. Especially, the range of low wavelengths is affected, increasing the beige-to-brownish color impression (*cf.* the color fields in the legend of Fig. 3b and c). Thus, the thickness of the $TaVO_x$ layer should be reduced as long as no negative impact on the charge transfer and the overall electrochemical switching characteristic is observed.

As for the key measures introduced before, the samples with varying layer thicknesses basically show a comparable trend in the charge density as function of the cycle number (*cf.* Fig. 3d). All films exhibit a decrease in capacity upon cycling. However, in comparison, this decrease is significantly more pronounced for the 200 and 300 nm thickness samples. This can be illustrated by the amount of charge density involved in the last cycle. For the 300 nm sample, we find a value of about 59.8 mC cm^{-2} in the eleventh cycle, which is only 76.4% of the initial cycle. This is comparable with the 200-nm layer, where the capacity remaining is 76% after the eleventh cycle. As mentioned before, the 100-nm-thick $TaVO_x$ layer retained 87.1% of its initial charge density. Further improvement may be made reducing the thickness to 75 nm. Here, the charge density is 26.5 mC cm^{-2} after the eleventh cycle, which is 90.8% compared to the first cycle. Thus, in terms of charge density, thinner $TaVO_x$ films may be preferred, as they exhibit better cycling stability. Taking a look at the coloration efficiency (*cf.* Fig. 3e), thinner layers seem superior as well. Here, for the samples with a thickness of 200 and 300 nm, respectively, the coloration efficiency increases significantly in the course of CV measurements. We observe an increase of approximately 0.3 cm^2 C^{-1} for both samples during the measurement. For the 75 and 100 nm thick films, respectively, a much less pronounced increase in the coloration

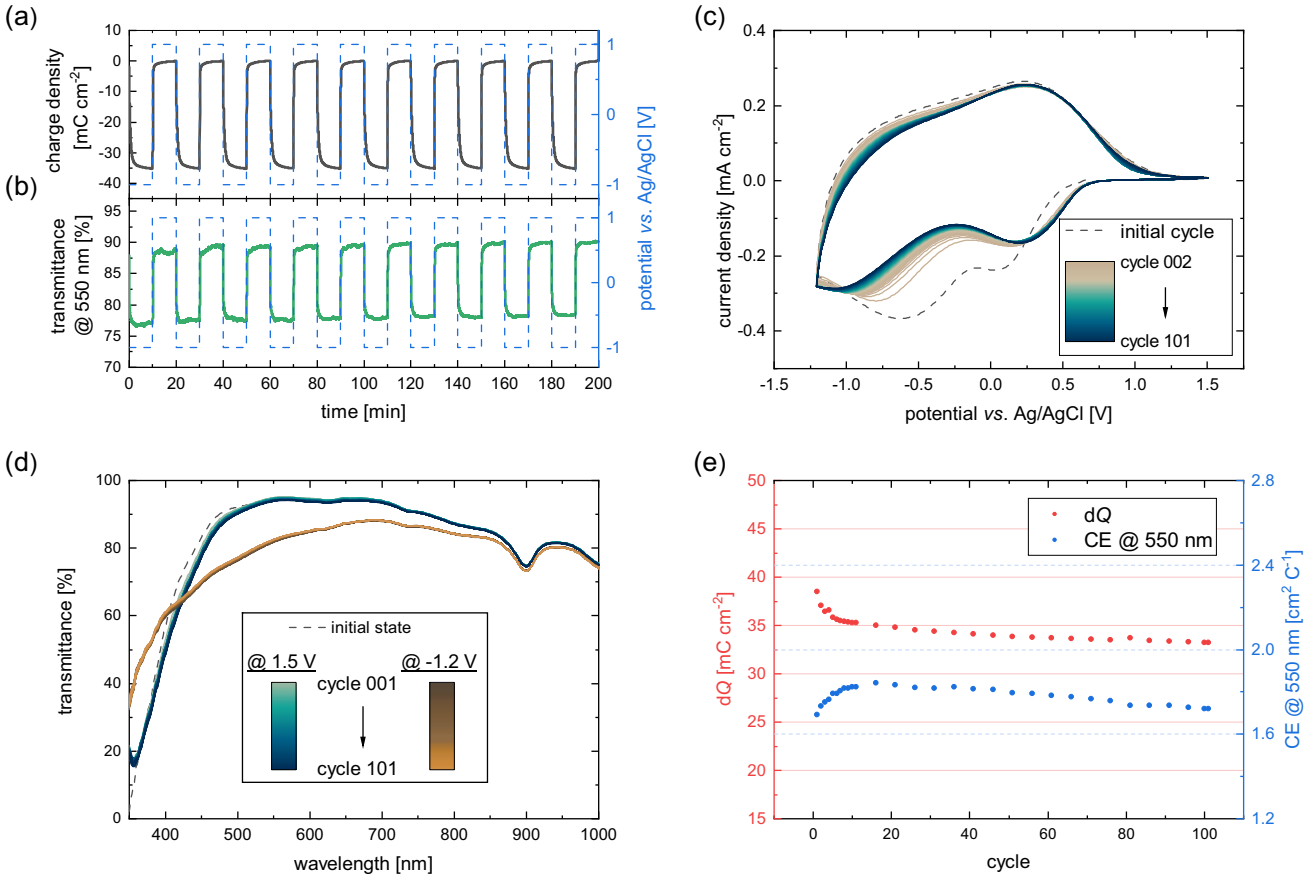

Figure 4 Time dependence of the charge density (**a**) and the transmittance at 550 nm (**b**) during ten cycles of a chronoamperometry measurement performed between the potentials of −1 and 1 V vs. Ag/AgCl, each applied for 10 min. Long-term study of 101 cyclic voltammograms (**c**) and the corresponding transmittance measurements at the potential reversal points (**d**). In addition, the determined charge density d*Q* and coloration efficiency CE at 550 nm are given (**e**).

efficiency is observed. Here, a typical change is only 0.1 $cm^2\ C^{-1}$ after completion of the entire measurement.

Taking into account switching kinetics and transmittance behavior, we conclude that $TaVO_x$ layers with thicknesses around 100 nm are suitable candidates for electrochromic applications.

Finally, we will discuss the suitability of rf-sputtered $TaVO_x$ layers in terms of switching times and long-term stability. Figure 4a shows a chronoamperometry (CA) measurement consisting of ten cycles. For every cycle, a voltage of −1 or 1 V *vs.* Ag/AgCl was applied for ten minutes each (*cf.* the ordinate to the right). The measurement was performed using a 100 nm thick $TaVO_x$ layer prepared with an O_2/Ar gas ratio of 10/40. Prior to the CA measurement, the coating has already passed eleven cycles of a CV measurement between −1.2 and 1.5 V *vs.* Ag/AgCl. The resulting (de-)intercalation steps of the charge density display a saturated profile at the end of the respective half cycles. A constant amount of charge density involved in the process results during the ten cycles. This corresponding value is about 35 mC cm^{-2}, consistent with what was observed in the CV (*cf.* Fig. 3d). Fig. 4b shows the optical transmittance at a wavelength of 550 nm and, thus, the cathodic electrochromic switching behavior as function of time. Within a cycle, there is a transmittance variation of about 12% between the states of maximum (de-)intercalation. The respective switching time for coloring and bleaching, which represents the time required for the system to complete 90% of the total switching step, is about 30 s in each case. This represents a suitable response time for the system.

As for the long-term cycling stability, we compare the results of 101 CV cycles in a potential range between −1.2 and 1.5 V *vs.* Ag/AgCl (*cf.* Fig. 4c–e). Fig. 4c shows the recorded voltammograms. Apart

from the initial cycle, the traces of the remaining voltammograms are analogous to the eleventh cycle discussed in context of Fig. 2a. Both the positions of the reduction and oxidation steps present and the current density at these potentials show good agreement. With increasing cycle number, however, a shift of the reduction signals is evident. Thus, the minimum of the first reduction step (between 0.1 and 0.2 V *vs*. Ag/AgCl) shifts towards a somewhat more positive potential. For the second reduction step (between −0.8 and −1.1 V *vs*. Ag/AgCl), the behavior is reversed and it shifts towards a more negative potential. As a result, the second reduction minimum approaches more and more the lower potential limit chosen in this work. Consequently, the last cycles of the measurement do not exhibit the complete reduction minimum and the current density of Li^+ deintercalation in the range between −0.5 and −1.0 V *vs*. Ag/AgCl decreases noticeably. The oxidation step at about 0.2 V *vs*. Ag/AgCl, however, has an almost constant potential position throughout all cycles. Figure 4d displays the transmittance at the potential reversal points corresponding to all CV measurements. In general, it can be observed that the initial state can be restored almost over the whole spectral range even after more than 100 cycles (*cf*. transmittance curves at 1.5 V *vs*. Ag/AgCl). Additionally, the optical transmittance in the intercalated state (at a potential of −1.2 V *vs*. Ag/AgCl) is also fully reproducible after each cycle. In terms of optical switching properties, the material therefore exhibits a high degree of stability within the first 100 cycles. This is also reflected in the key measures dQ and CE (*cf*. Fig. 4e). Since the enclosed area of the voltammograms is reduced upon cycling, the charge density involved per cycle decreases slightly as well. In the first cycle, we observe a charge density of 38.5 mC cm^{-2}. After 101 cycles, it is only 33.2 mC cm^{-2}, which represents 86.2%. However, since the strongest decrease in charge density occurs within the first ten cycles, cycle 101 still exhibits 94.1% of the charge density of the tenth cycle. Thus, after a first loss of performance, a high reversibility over all further cycles is evident with regard to optical switching. The corresponding coloration efficiency at 550 nm stays between 1.7 and 1.8 cm^2 C^{-1} over the wide range of the measurement.

Conclusion

We deposit tantalum vanadium oxide films by rf-magnetron sputtering at different O_2/Ar compositions of the process gas. All samples exhibit the mixed anodic/cathodic electrochromic behaviour, known from binary V_2O_5. However, our ternary $TaVO_x$ films are more suitable for use as a counter electrode in a smart window due to a higher color neutrality. Furthermore, we find low oxygen sputter conditions to yield layers with improved electrochemical properties. We state an optimized thickness of approximately 100 nm, as those layers combine suitable electrochemical switching kinetics with adequate optical properties, and determine optical switching times for coloring/bleaching of less than 30 s. Simultaneously, a total charge density of about 35 mC cm^{-2} per cycle is achieved. Electrochemical stability as well as optical reversibility is given even after more than 100 cycles. Nevertheless, the exact composition as well as the structure of the ternary mixture remains unclear. Similarly, there is a lack of knowledge of the metal species present in the (de-)intercalated states. This has prompted us to plan further investigations, focusing on X-ray photoelectron spectroscopic studies. Based on the results presented here, sputtered $TaVO_x$ may be an alternative to common ion storage layer materials and pave the way for obtaining beneficial performance in future electrochromic devices.

Acknowledgements

We thank D. Schlettwein and T. H. Q. Nguyen for fruitful discussions and valuable help in the experimental setup. The work of M. Gies was funded by the DFG via the RTG (Research Training Group) 2204 “Substitute Materials for Sustainable Energy Technologies.”

Funding

Open Access funding enabled and organized by Projekt DEAL.

Declarations

Conflict of interest The authors declare that they have no conflict of interest.

Supplementary Information: The online version contains supplementary material available at https://doi.org/10.1007/s10853-022-07408-0.

References

[1] bp (2021) Statistical Review of World Energy, 70th edition.

[2] Architecture 2030 (2022) Why the building sector? https://architecture2030.org/why-the-building-sector/. Accessed 10 Mar 2022.

[3] International Energy Agency (2022) Cooling–analysis–IEA. https://www.iea.org/reports/cooling. Accessed 10 Mar 2022.

[4] Sequeira CAC, Santos DMF (2010) Tungsten oxide electrochromic windows with lithium polymer electrolytes. J Electrochem Soc 157(6):J202. https://doi.org/10.1149/1.3364865

[5] Panero S, Scrosati B, Baret M, Cecchini B, Masetti E (1995) Electrochromic windows based on polyaniline, tungsten oxide and gel electrolytes. Sol Energy Mater Sol Cells 39(2–4):239–246. https://doi.org/10.1016/0927-0248(95)00042-9

[6] Granqvist CG (2014) Electrochromics for smart windows: oxide-based thin films and devices. Thin Solid Films 564:1–38. https://doi.org/10.1016/j.tsf.2014.02.002

[7] Gies M, Michel F, Lupó C, Schlettwein D, Becker M, Polity A (2021) Electrochromic switching of tungsten oxide films grown by reactive ion-beam sputter deposition. J Mater Sci 56(1):615–628. https://doi.org/10.1007/s10853-020-05321-y

[8] Granqvist C (1999) Progress in electrochromics: tungsten oxide revisited. Electrochim Acta 44(18):3005–3015. https://doi.org/10.1016/S0013-4686(99)00016-X

[9] Granqvist C (2000) Electrochromic tungsten oxide films: review of progress 1993–1998. Sol Energy Mater Sol Cells 60(3):201–262. https://doi.org/10.1016/S0927-0248(99)00088-4

[10] Niklasson GA, Granqvist CG (2007) Electrochromics for smart windows: thin films of tungsten oxide and nickel oxide, and devices based on these. J Mater Chem 17(2):127–156. https://doi.org/10.1039/B612174H

[11] Deb SK (1969) A novel electrophotographic system. Appl Opt 8(S1):192. https://doi.org/10.1364/AO.8.S1.000192

[12] Deb SK (1973) Optical and photoelectric properties and colour centres in thin films of tungsten oxide. Phil Mag 27(4):801–822. https://doi.org/10.1080/14786437308227562

[13] Wu W, Wang M, Ma J, Cao Y, Deng Y (2018) Electrochromic metal oxides: recent progress and prospect. Adv Electron Mater 4(8):1800185. https://doi.org/10.1002/aelm.201800185

[14] Gupta J, Shaik H, Kumar KN (2021) A review on the prominence of porosity in tungsten oxide thin films for electrochromism. Ionics 27(6):2307–2334. https://doi.org/10.1007/s11581-021-04035-8

[15] Zeb S, Sun G, Nie Y, Xu H, Cui Y, Jiang X (2021) Advanced developments in nonstoichiometric tungsten oxides for electrochromic applications. Mater Adv 2(21):6839–6884. https://doi.org/10.1039/d1ma00418b

[16] Mehmood A, Long X, Haidry AA, Zhang X (2020) Trends in sputter deposited tungsten oxide structures for electrochromic applications: a review. Ceram Int 46(15):23295–23313. https://doi.org/10.1016/j.ceramint.2020.06.035

[17] Tang K, Zhang Y, Shi Y, Cui J, Shu X, Wang Y, Liu J, Wang J, Tan HH, Wu Y (2018) Preparation of V 2 O 5 dot-decorated WO 3 nanorod arrays for high performance multi-color electrochromic devices. J Mater Chem C 6(45):12206–12216. https://doi.org/10.1039/C8TC04247K

[18] Lee SJ, Choi DS, Kang SH, Yang WS, Nahm S, Han SH, Kim T (2019) VO 2 /WO 3 -Based hybrid smart windows with thermochromic and electrochromic properties. ACS

Sustain Chem Eng 7(7):7111–7117. https://doi.org/10.1021/acssuschemeng.9b00052

[19] Guo Q, Zhao X, Li Z, Wang B, Wang D, Nie G (2020) High performance multicolor intelligent supercapacitor and its quantitative monitoring of energy storage level by electrochromic parameters. ACS Appl Energy Mater 3(3):2727–2736. https://doi.org/10.1021/acsaem.9b02392

[20] Wang J-L, Liu J-W, Sheng S-Z, He Z, Gao J, Yu S-H (2021) Manipulating nanowire assemblies toward multicolor transparent electrochromic device. Nano Lett 21(21):9203–9209. https://doi.org/10.1021/acs.nanolett.1c03061

[21] Rai V, Singh RS, Blackwood DJ, Zhili D (2020) A review on recent advances in electrochromic devices: a material approach. Adv Eng Mater 22(8):2000082. https://doi.org/10.1002/adem.202000082

[22] Bogati S, Basnet R, Georg A (2019) Iridium oxide catalyst for hybrid electrochromic device based on tetramethylthiourea (TMTU) redox electrolyte. Sol Energy Mater Sol Cells 189:206–213. https://doi.org/10.1016/j.solmat.2018.09.026

[23] Ito S, Abe Y, Kawamura M, Kim KH (2015) Electrochromic properties of iridium oxide thin films prepared by reactive sputtering in O 2 or H 2 O atmosphere. J Vac Sci Technol, B: Nanotechnol Microelectron: Mater, Process, Meas, Phenom 33(4):41204. https://doi.org/10.1116/1.4923227

[24] Zhang H, Liu S, Xu T, Xie W, Chen G, Liang L, Gao J, Cao H (2021) Aluminum-ion-intercalation nickel oxide thin films for high-performance electrochromic energy storage devices. J Mater Chem C 9(48):17427–17436. https://doi.org/10.1039/d1tc04240h

[25] Patel KJ, Bhatt GG, Ray JR, Suryavanshi P, Panchal CJ (2017) All-inorganic solid-state electrochromic devices: a review. J Solid State Electrochem 21(2):337–347. https://doi.org/10.1007/s10008-016-3408-z

[26] Dong D, Wang W, Rougier A, Dong G, Da Rocha M, Presmanes L, Zrikem K, Song G, Diao X, Barnabé A (2018) Life-cycling and uncovering cation-trapping evidence of a monolithic inorganic electrochromic device: glass/ITO/WO3/LiTaO3/NiO/ITO. Nanoscale 10(35):16521–16530. https://doi.org/10.1039/C8NR02267D

[27] Arvizu MA, Qu H-Y, Cindemir U, Qiu Z, Rojas-González EA, Primetzhofer D, Granqvist CG, Österlund L, Niklasson GA (2019) Electrochromic WO_3 thin films attain unprecedented durability by potentiostatic pretreatment. J Mater Chem A 7(6):2908–2918. https://doi.org/10.1039/C8TA09621J

[28] Wen-Cheun AuB, Chan K-Y, Knipp D (2019) Effect of film thickness on electrochromic performance of sol-gel deposited tungsten oxide (WO_3). Opt Mater 94:387–392. https://doi.org/10.1016/j.optmat.2019.05.051

[29] Bahlawane N, Lenoble D (2014) Vanadium oxide compounds: structure, properties, and growth from the gas phase. Chem Vap Deposition 20(7–9):299–311. https://doi.org/10.1002/cvde.201400057

[30] Crociani L, Carta G, Natali M, Rigato V, Rossetto G (2011) MOCVD of vanadium oxide films with a novel vanadium(III) precursor. Chem Vap Deposition 17(1–3):6–8. https://doi.org/10.1002/cvde.201004291

[31] Drosos C, Jia C, Mathew S, Palgrave RG, Moss B, Kafizas A, Vernardou D (2018) Aerosol-assisted chemical vapor deposition of V_2O_5 cathodes with high rate capabilities for magnesium-ion batteries. J Power Sources 384:355–359. https://doi.org/10.1016/j.jpowsour.2018.02.074

[32] Louloudakis D, Vernardou D, Spanakis E, Katsarakis N, Koudoumas E (2013) Electrochemical properties of vanadium oxide coatings grown by APCVD on glass substrates. Surf Coat Technol 230:186–189. https://doi.org/10.1016/j.surfcoat.2013.06.054

[33] Partlow DP, Gurkovich SR, Radford KC, Denes LJ (1991) Switchable vanadium oxide films by a sol-gel process. J Appl Phys 70(1):443–452. https://doi.org/10.1063/1.350272

[34] Liberatore M, Decker F, Šurca Vuk A, Orel B, Dražič G (2006) Effect of the organic–inorganic template ICS-PPG on sol–gel deposited V_2O_5 electrochromic thin film. Sol Energy Mater Sol Cells 90(4):434–443. https://doi.org/10.1016/j.solmat.2005.04.035

[35] Song GY, Oh C, Sinha S, Son J, Heo J (2017) Facile phase control of multivalent vanadium oxide thin films (V_2O_5 and VO_2) by atomic layer deposition and postdeposition annealing. ACS Appl Mater Interfaces 9(28):23909–23917. https://doi.org/10.1021/acsami.7b03398

[36] Mattelaer F, Geryl K, Rampelberg G, Dobbelaere T, Dendooven J, Detavernier C (2016) Atomic layer deposition of vanadium oxides for thin-film lithium-ion battery applications. RSC Adv 6(115):114658–114665. https://doi.org/10.1039/C6RA25742A

[37] Bhardwaj D, Singh DK, Krupanidhi SB, Umarji AM (2020) Fabrication of smooth thin film of vanadium oxides (VO_x) using pulsed laser deposition. Appl Phys A. https://doi.org/10.1007/s00339-020-3310-5

[38] Burdis MS (1997) Properties of sputtered thin films of vanadium–titanium oxide for use in electrochromic windows. Thin Solid Films 311(1–2):286–298. https://doi.org/10.1016/S0040-6090(97)00724-4

[39] Benmoussa M, Outzourhit A, Bennouna A, Ameziane E (2002) Electrochromism in sputtered V_2O_5 thin films: structural and optical studies. Thin Solid Films 405(1–2):11–16. https://doi.org/10.1016/S0040-6090(01)01734-5

[40] Lim JW, Yoo SJ, Park SH, Yun SU, Sung Y-E (2009) High electrochromic performance of co-sputtered vanadium–titanium oxide as a counter electrode. Sol Energy Mater Sol Cells 93(12):2069–2074. https://doi.org/10.1016/j.solmat.2009.03.008

[41] Ottaviano L, Pennisi A, Simone F, Salvi AM (2004) RF sputtered electrochromic V_2O_5 films. Opt Mater 27(2):307–313. https://doi.org/10.1016/j.optmat.2004.04.001

[42] Panagopoulou M, Vernardou D, Koudoumas E, Tsoukalas D, Raptis YS (2017) Oxygen and temperature effects on the electrochemical and electrochromic properties of rf-sputtered V_2O_5 thin films. Electrochim Acta 232:54–63. https://doi.org/10.1016/j.electacta.2017.02.128

[43] Miyazaki H (1999) Electrochemical evaluation of oriented vanadium oxide films deposited by reactive rf magnetron sputtering. Solid State Ionics 122(1–4):223–229. https://doi.org/10.1016/S0167-2738(99)00022-3

[44] Wang Y, Cao G (2006) Synthesis and enhanced intercalation properties of nanostructured vanadium oxides. Chem Mater 18(12):2787–2804. https://doi.org/10.1021/cm052765h

[45] Lindström R, Maurice V, Groult H, Perrigaud L, Zanna S, Cohen C, Marcus P (2006) Li-intercalation behaviour of vanadium oxide thin film prepared by thermal oxidation of vanadium metal. Electrochim Acta 51(23):5001–5011. https://doi.org/10.1016/j.electacta.2006.01.049

[46] Delmas C, Brèthes S, Ménétrier M (1991) ω-$Li_xV_2O_5$–a new electrode material for rechargeable lithium batteries. J Power Sources 34(2):113–118. https://doi.org/10.1016/0378-7753(91)85030-Z

[47] Delmas C, Cognac-Auradou H, Cocciantelli J, Ménétrier M, Doumerc J (1994) The $Li_xV_2O_5$ system: an overview of the structure modifications induced by the lithium intercalation. Solid State Ionics 69(3–4):257–264. https://doi.org/10.1016/0167-2738(94)90414-6

[48] Yan B, Li X, Fu X, Zhang L, Bai Z, Yang X (2020) An elaborate insight of lithiation behavior of V_2O_5 anode. Nano Energy 78:105233. https://doi.org/10.1016/j.nanoen.2020.105233

[49] Mattelaer F, Geryl K, Rampelberg G, Dendooven J, Detavernier C (2017) Amorphous and crystalline vanadium oxides as high-energy and high-power cathodes for three-dimensional thin-film lithium ion batteries. ACS Appl Mater Interfaces 9(15):13121–13131. https://doi.org/10.1021/acsami.6b16473

[50] Liu Y, Clark M, Zhang Q, Yu D, Liu D, Liu J, Cao G (2011) V_2O_5 Nano-electrodes with high power and energy densities for thin film Li-Ion batteries. Adv Energy Mater 1(2):194–202. https://doi.org/10.1002/aenm.201000037

[51] Gies A, Pecquenard B, Benayad A, Martinez H, Gonbeau D, Fuess H, Levasseur A (2008) Effect of silver co-sputtering on V_2O_5 thin films for lithium microbatteries. Thin Solid Films 516(21):7271–7281. https://doi.org/10.1016/j.tsf.2007.12.165

[52] Chen P, Zheng G, Guo G, Wang Z, Tang J, Li S, Wen Z, Ji S, Sun J (2019) Ce-doped V_2O_5 microspheres with improved electrochemical performance for high-power rechargeable lithium ion batteries. J Alloy Compd 784:574–583. https://doi.org/10.1016/j.jallcom.2018.12.373

[53] Zeng H, Liu D, Zhang Y, See KA, Jun Y-S, Wu G, Gerbec JA, Ji X, Stucky GD (2015) Nanostructured Mn-Doped V_2O_5 cathode material fabricated from Layered vanadium jarosite. Chem Mater 27(21):7331–7336. https://doi.org/10.1021/acs.chemmater.5b02840

[54] Wu G, Du K, Xia C, Kun X, Shen J, Zhou B, Wang J (2005) Optical absorption edge evolution of vanadium pentoxide films during lithium intercalation. Thin Solid Films 485(1–2):284–289. https://doi.org/10.1016/j.tsf.2005.03.039

[55] Cogan SF, Nguyen NM, Perrotti SJ, Rauh RD (1989) Optical properties of electrochromic vanadium pentoxide. J Appl Phys 66(3):1333–1337. https://doi.org/10.1063/1.344432

[56] Fujita Y, Miyazaki K, Tatsuyama C (1985) On the electrochromism of evaporated V_2O_5 Films. Jpn J Appl Phys 24:1082–1086. https://doi.org/10.1143/JJAP.24.1082

[57] Colton RJ, Guzman AM, Rabalais JW (1978) Electrochromism in some thin-film transition-metal oxides characterized by x-ray electron spectroscopy. J Appl Phys 49(1):409–416. https://doi.org/10.1063/1.324349

[58] Picardi G, Varsano F, Decker F, Opara-Krasovec U, Surca A, Orel B (1999) Electrochemical characterization of optically passive $CeVO_4$ counterelectrodes. Electrochim Acta 44(18):3157–3164. https://doi.org/10.1016/S0013-4686(99)00033-X

[59] Šurca A, Benčič S, Orel B, Pihlar B (1999) Spectroelectrochemical studies of V/Ti-, V/Ti/Zr- and V/Ti/Ce-oxide counter-electrode films. Electrochim Acta 44(18):3075–3084. https://doi.org/10.1016/S0013-4686(99)00023-7

[60] Dalavi DS, Bhosale AK, Desai RS, Patil PS (2021) Energy efficient electrochromic smart windows based on highly stable CeO_2-V_2O_5 optically passive counter electrode. Mater Today: Proc 43:2702–2706. https://doi.org/10.1016/j.matpr.2020.06.146

[61] Cogan SF, Rauh RD, Nguyen NM, Plante TD, Westwood JD (1993) Electrochromism in Nb-V and Cr-V mixed-oxides. J Electrochem Soc 140(1):112–115. https://doi.org/10.1149/1.2056069

[62] Bae J-W, Koo B-R, Ahn H-J (2019) Fe doping effect of vanadium oxide films for enhanced switching electrochromic

performances. Ceram Int 45(6):7137–7142. https://doi.org/10.1016/j.ceramint.2018.12.219

[63] Jin A, Chen W, Zhu Q, Yang Y, Volkov VL, Zakharova GS (2009) Structural and electrochromic properties of molybdenum doped vanadium pentoxide thin films by sol–gel and hydrothermal synthesis. Thin Solid Films 517(6):2023–2028. https://doi.org/10.1016/j.tsf.2008.10.001

[64] Li Y-M, Kudo T (1995) Properties of mixed-oxide MoO_3/V_2O_5 electrochromic films coated from peroxo-polymolybdovanadate solutions. Sol Energy Mater Sol Cells 39(2–4):179–190. https://doi.org/10.1016/0927-0248(95)00050-X

[65] Li Y-M, Kudo T (1996) Lithium intercalation dynamics of spin-coated amorphous $Mo_{0.5}V_{0.5}O_{2.75}$ thin film. Solid State Ionics 86–88:1295–1299. https://doi.org/10.1016/0167-2738(96)00304-9

[66] Mjejri I, Gaudon M, Rougier A (2019) Mo addition for improved electrochromic properties of V_2O_5 thick films. Sol Energy Mater Sol Cells 198:19–25. https://doi.org/10.1016/j.solmat.2019.04.010

[67] Westphal TM, Cholant CM, Azevedo CF, Moura EA, Da Silva DL, Lemos RM, Pawlicka A, Gündel A, Flores WH, Avellaneda CO (2017) Influence of the Nb_2O_5 doping on the electrochemical properties of V_2O_5 thin films. J Electroanal Chem 790:50–56. https://doi.org/10.1016/j.jelechem.2017.02.014

[68] Wang S, Goonetilleke D, Sharma N (2018) Electrochemical modification of negative thermal expansion materials in the $Ta_xNb_{1-x}VO_5$ series. Inorg Chem 57(17):10633–10639. https://doi.org/10.1021/acs.inorgchem.8b01280

[69] Amarilla JM, Casal B, Galván JC, Ruiz-Hitzky E (1992) Lithium intercalation in $Ta_xNb_{1-x}VO_5$ mixed oxides. MSF 91–93:153–158. https://doi.org/10.4028/www.scientific.net/MSF.91-93.153

[70] Amarilla JM, Casal B, Galvan JC, Ruiz-Hitzky E (1992) Lithium-niobium vanadium oxide and lithium-tantalum vanadium oxide, MVO_5, bronzes. Chem Mater 4(1):62–67. https://doi.org/10.1021/cm00019a015

[71] Avellaneda CO (2007) Electrochromic performance of sol–gel deposited V_2O_5: Ta films. Mater Sci Eng, B 138(2):118–122. https://doi.org/10.1016/j.mseb.2006.06.007

[72] Avellaneda CO, Bulhões LO (2006) Optical and electrochemical properties of V_2O_5: Ta Sol-Gel thin films. Sol Energy Mater Sol Cells 90(4):444–451. https://doi.org/10.1016/j.solmat.2005.04.031

[73] Burdis M, Siddle J, Batchelor R, Gallego J (1998) $V_{0.50}$-$Ti_{0.50}Ox$ thin films as counterelectrodes for electrochromic devices. Solar Energy Mater. Solar Cells 54(1–4):93–98. https://doi.org/10.1016/S0927-0248(98)00059-2

[74] Kumar A, Sahay PP (2020) Influence of Ti doping on the microstructural and electrochromic properties of dip-coated nanocrystalline V_2O_5 thin films. J Sol-Gel Sci Technol 95(1):34–51. https://doi.org/10.1007/s10971-020-05298-9

[75] Nagase K, Shimizu Y, Miura N, Yamazoe N (1992) Electrochromism of vanadium-titanium oxide thin films prepared by spin-coating method. Appl Phys Lett 61(3):243–245. https://doi.org/10.1063/1.107956

[76] Panagopoulou M, Vernardou D, Koudoumas E, Tsoukalas D, Raptis YS (2019) Tungsten doping effect on V_2O_5 thin film electrochromic performance. Electrochim Acta 321:134743. https://doi.org/10.1016/j.electacta.2019.134743